Paolo P. Provenzano, David R. Inman, Kevin W. Eliceiri, and Patricia J. Keely

MATRIX DENSITY-INDUCED MECHANOREGULATION OF BREAST CELL PHENOTYPE, SIGNALING, AND GENE EXPRESSION THROUGH A FAK-ERK LINKAGE

SUPPLEMENTARY INFORMATION

This file contains the following items:

1. Supplementary Figure S1-S9
2. Supplementary Materials and Methods
3. Supplementary Discussion Text

Provenzano et al., Supp. Figure S1:

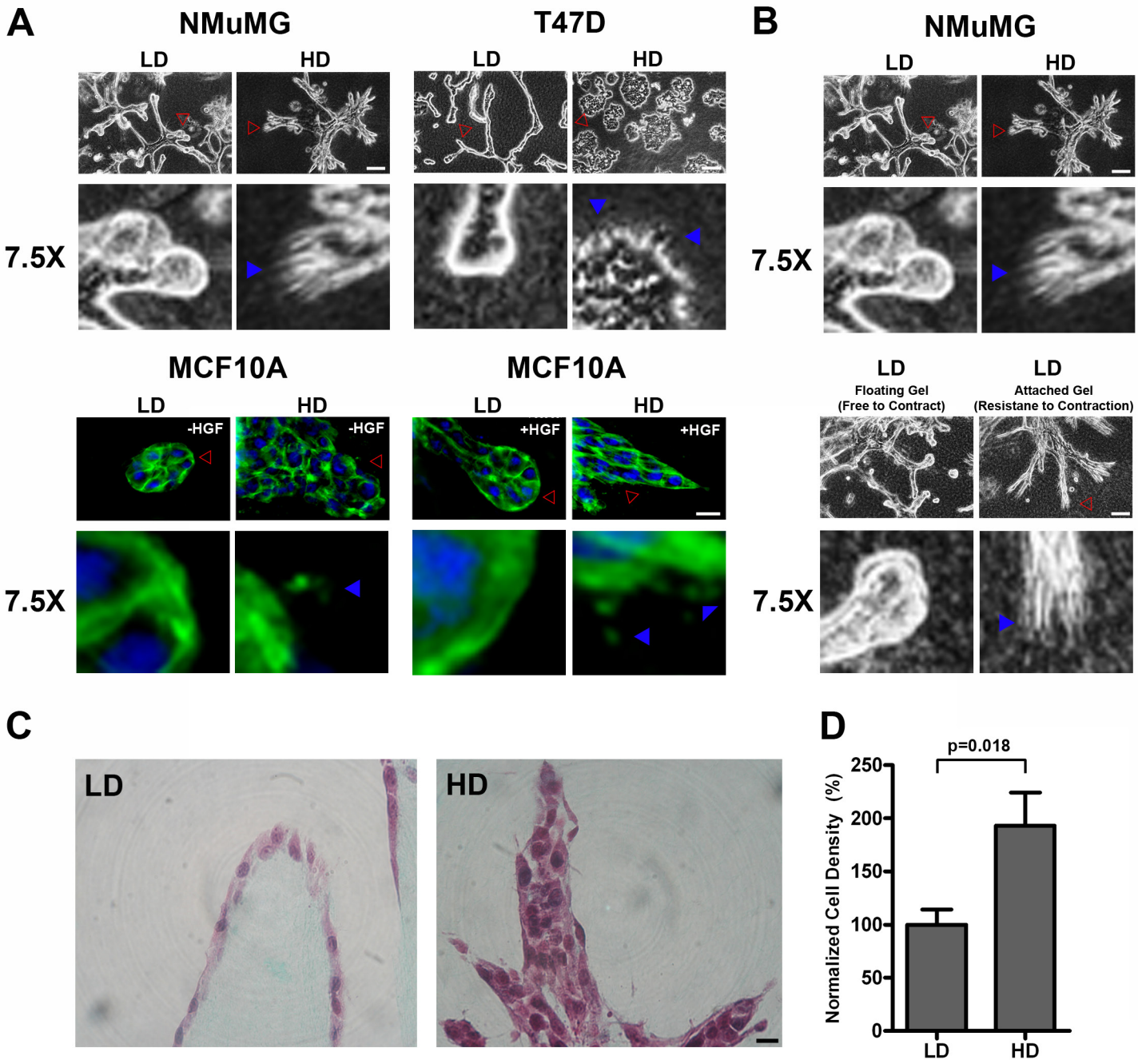

Supplementary Figure S1:

(A) Representative micrographs of mammary epithelial cells in low-density (LD) and high-density (HD) matrices, optimized for each cell type – See Experimental Procedures. For both mouse and human cells, increasing collagen matrix density disrupted proper tubule formation and resulted in larger and more invasive colonies. Blue arrowheads highlight examples of increased membrane protrusion for each cell type cultured under HD conditions. The magnifide regions (7.5X) are indicated with red arrowheads. In order to promote tubulogenesis in MCF10A cells, 50ng/mL HGF was added to the media. Addition of HGF is not necessary for NMuMG or T47D cells. Bars: NMuMG and T47D = 100 μm; MCF10A = 20 μm

(B) Representative micrographs of NMuMG seeded into LD collagen matrices that were allowed to freely contract and undergo tubulogenesis (bottom left) or constrained at the matrix boundary to provide increased resistance to cell contraction (bottom right). Note that increasing resistance to cell contraction recapitulated the HD phenotype (top panels). Bar = 100 μm

(C) Representative histology (Trichrome staining) of NMuMG mammary epithelial cells cultured in LD or HD matrices for 7 days showing loss of luminal differentiation and increased cell density in HD culture.

(D) Quantitative analysis of the number of cells per field for colonies in LD and HD matrices,(expressed as a normalized percent) showing significantly more cells in HD colonies.

Provenzano et al., Supp. Figure S2

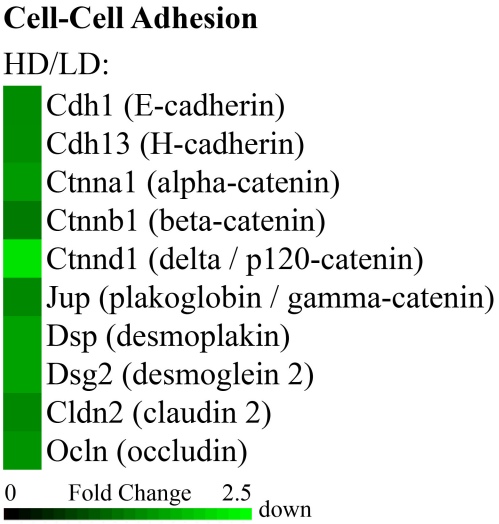

Supplementary Figure S2:
Heat map of transcripts associated with cell-cell adhesion showing a significant decrease in markers for cell junctions in cells within HD matrices.

Provenzano et al., Supp. Figure S3

The high-density phenotype is not due to increased local ligand (collagen) density at the cell membrane

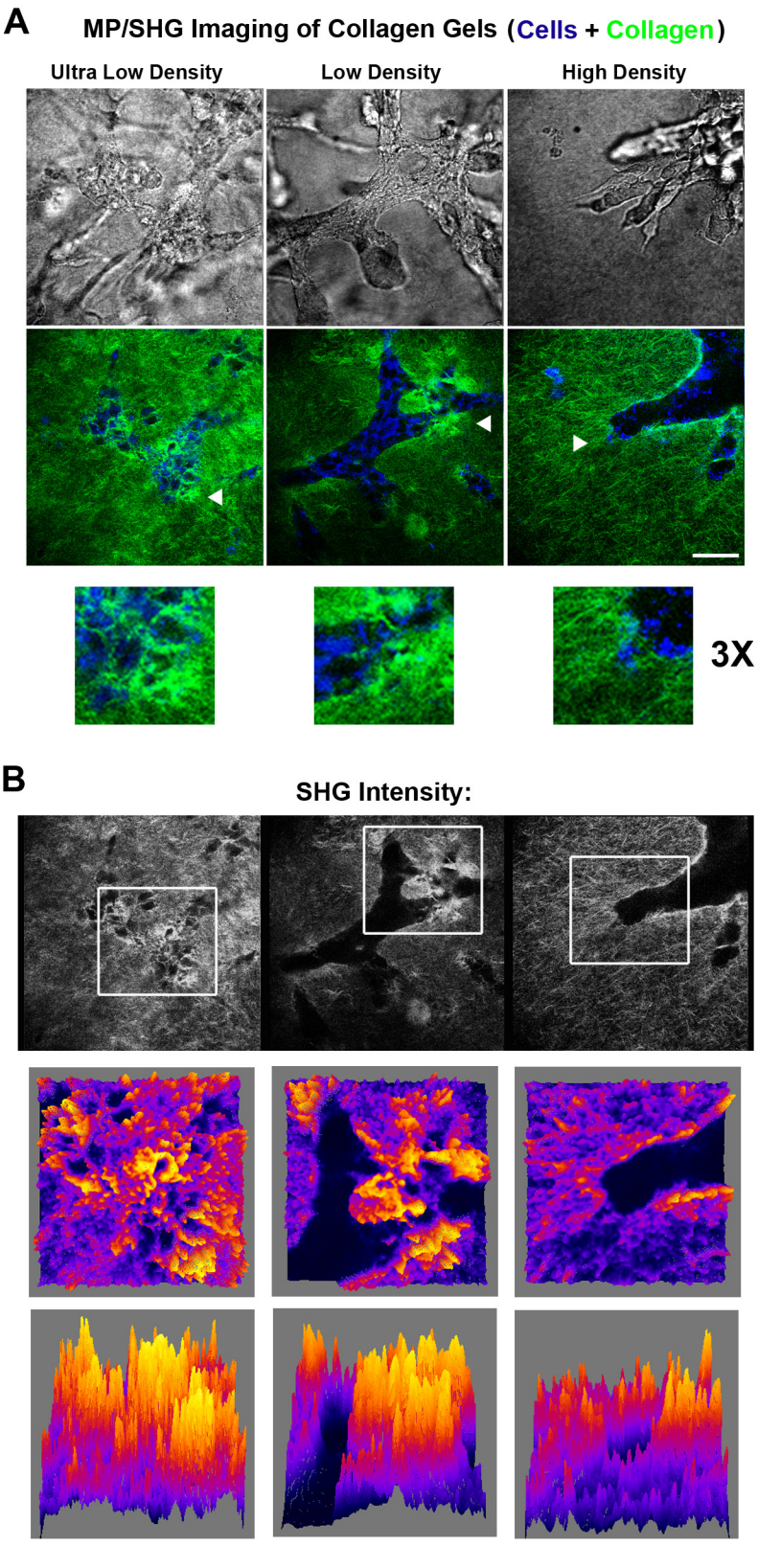

Supplementary Figure S3:

It is important to note that increased ligand concentration is unlikely to explain the HD phenotype, as cells in the attached LD matrices exhibit the same invasive phenotype as HD gels (Fig 1B, Supp. Fig. S1), even though there is no increase in ligand concentration in an attached LD matrix when compared to a floating LD matrix. Moreover, as shown in Supp. Fig. S3, lower-density matrices are more contractible than higher-density matrices. As a result, more collagen is present locally at the cell-matrix interface in lower density matrices. This was established and quantified by second harmonic generation (SHG) imaging of collagen, in which the signal intensity scales linearly with, and is a good measure of, collagen concentration (Brown et al., 2003). Importantly, although SHG imaging demonstrated that more collagen is present at the cell surface in more contracted matrices (Supp. Fig. S3), these cells did not transition to the invasive phenotype associated with HD matrices, indicating that increased local collagen ligand for integrin binding is not the dominating factor. Hence, the phenotype for cells in HD matrices does not appear to be due to increased presence of collagen ligand, but due to increased extracellular matrix stiffness associated with HD matrices. (A) Representative micrographs of transmitted light (top) and live cell multiphoton excitation (MP) and second harmonic generation (SHG; middle) of NMuMG cells (endogenous fluorescence: pseudo-colored blue) in contracted collagen matrices (SHG: pseudo-colored green) of varying density after 7 days. Arrowheads indicate regions magnifide (3X) in the bottom panel of A. Note the increase in local collagen signal at the cell-ECM interface as matrix contraction increases with lower density matrices. (B) Surface SHG intensity maps of collagen matrices of varying density from A. Regions that are magnifide and analyzed are identified with a bounding box (top). Intensity maps viewed from the z-direction (middle) and from an angle ~30 degrees off normal (bottom), where intensity is mapped from low (blue) to high (yellow), clearly indicates increased collagen near epithelial cells in lower density matrices, supporting the conclusion that the high density phenotype is not due to increased collagen binding, but is a result of mechanical reguation. Bar = 25 μm

Provenzano et al., Supp. Figure S4:

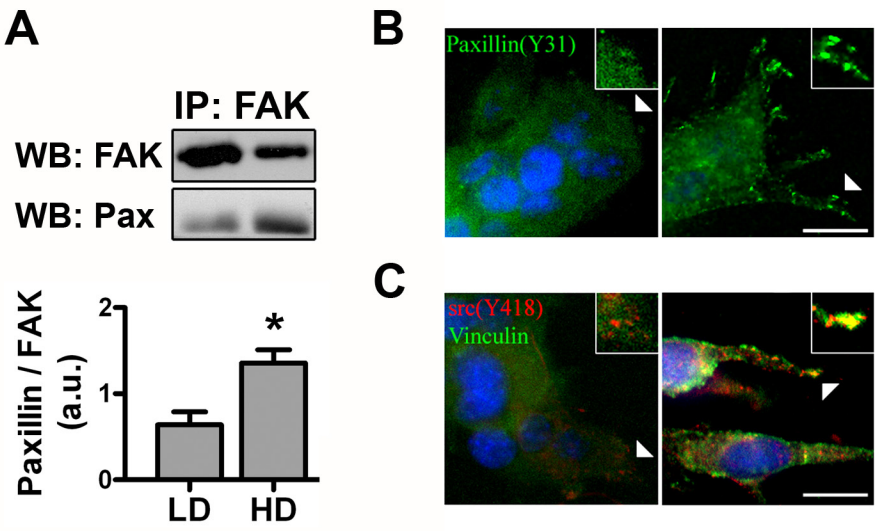

Supplementary Figure S4:
(A) Western blot analysis of Paxillin (Pax) protein that co-precipitated with immunoprecipitated FAK, showing increased FAK-Pax association in cells within stiffer HD matrices (n = 3; *p=0.029; mean ± SEM). LD = low density; HD = high density matrix.
(B) Immunofluorescence analysis of NMuMG cells in LD and HD collagen matrices showing active (phosphorylated at Y31) Paxillin localized to 3D-matrix adhesions. Bar = 10 μm
(C) Immunofluorescence analysis of increased pSrc(Y418) localized to 3D matrix adhesions in HD collagen matrices. Bar = 10 μm

Provenzano et al., Supp. Figure S5

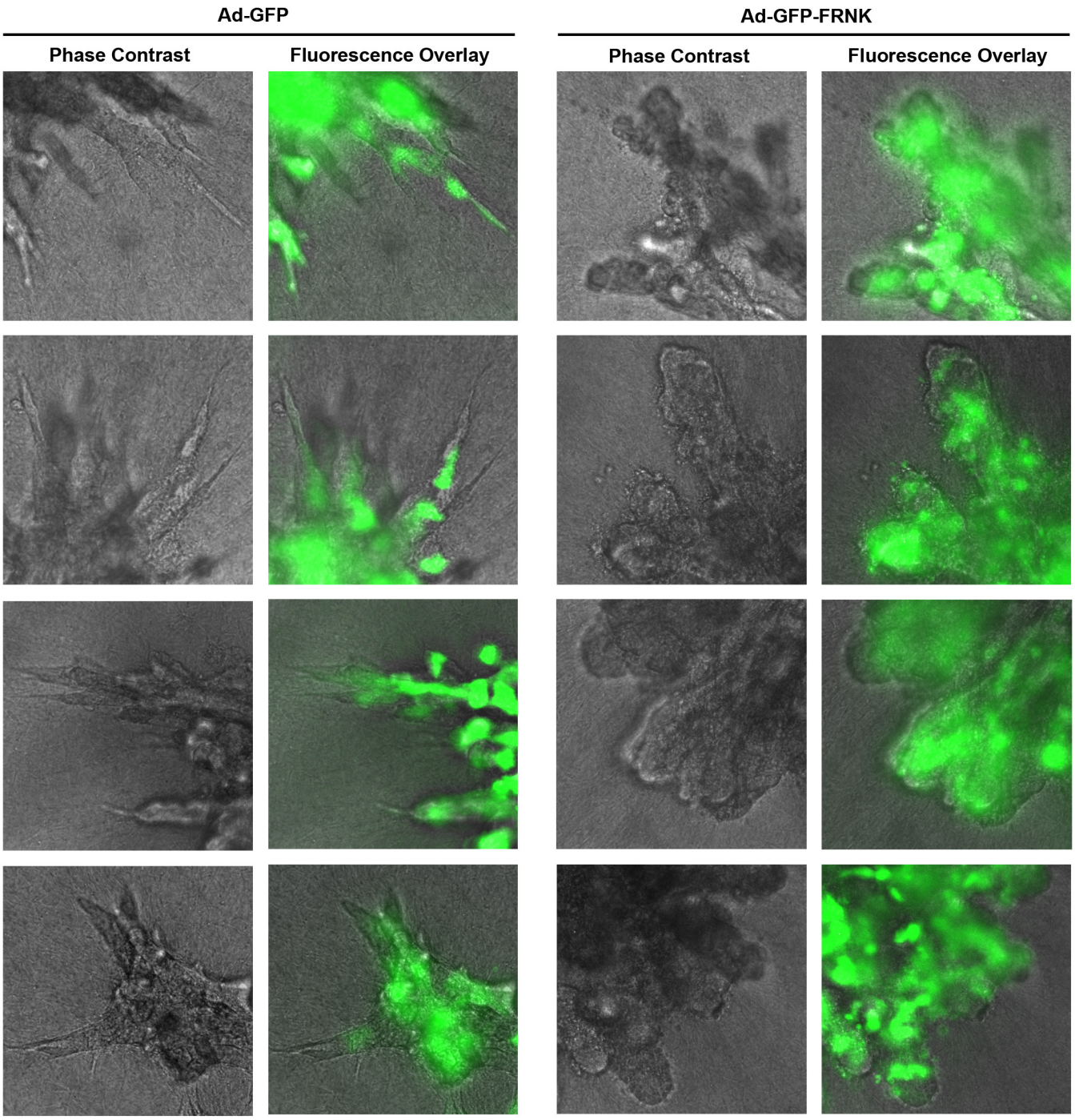

Supplementary Figure S5:
Inhibition of FAK activity with FRNK, a dominant-negative C-terminal region of FAK, reverted the invasive phenotype resulting from stiff HD matrices. NMuMG cells cultured in HD matrices for 7 days developed the invasive phenotype associated with stiff microenvironments (Left Panels). Adenoviral delivery of FRNK (expressing GFP as a marker of infection) resulted in reversion of the invasive phenotype after 24 hours (Right Panels). Each of the four representative panels for control (GFP) or treated (GFP-FRNK) are from separate paired cultures.

Provenzano et al., Supp. Figure S6

Enriched Transcripts Differentially Expressed by Matrix Density

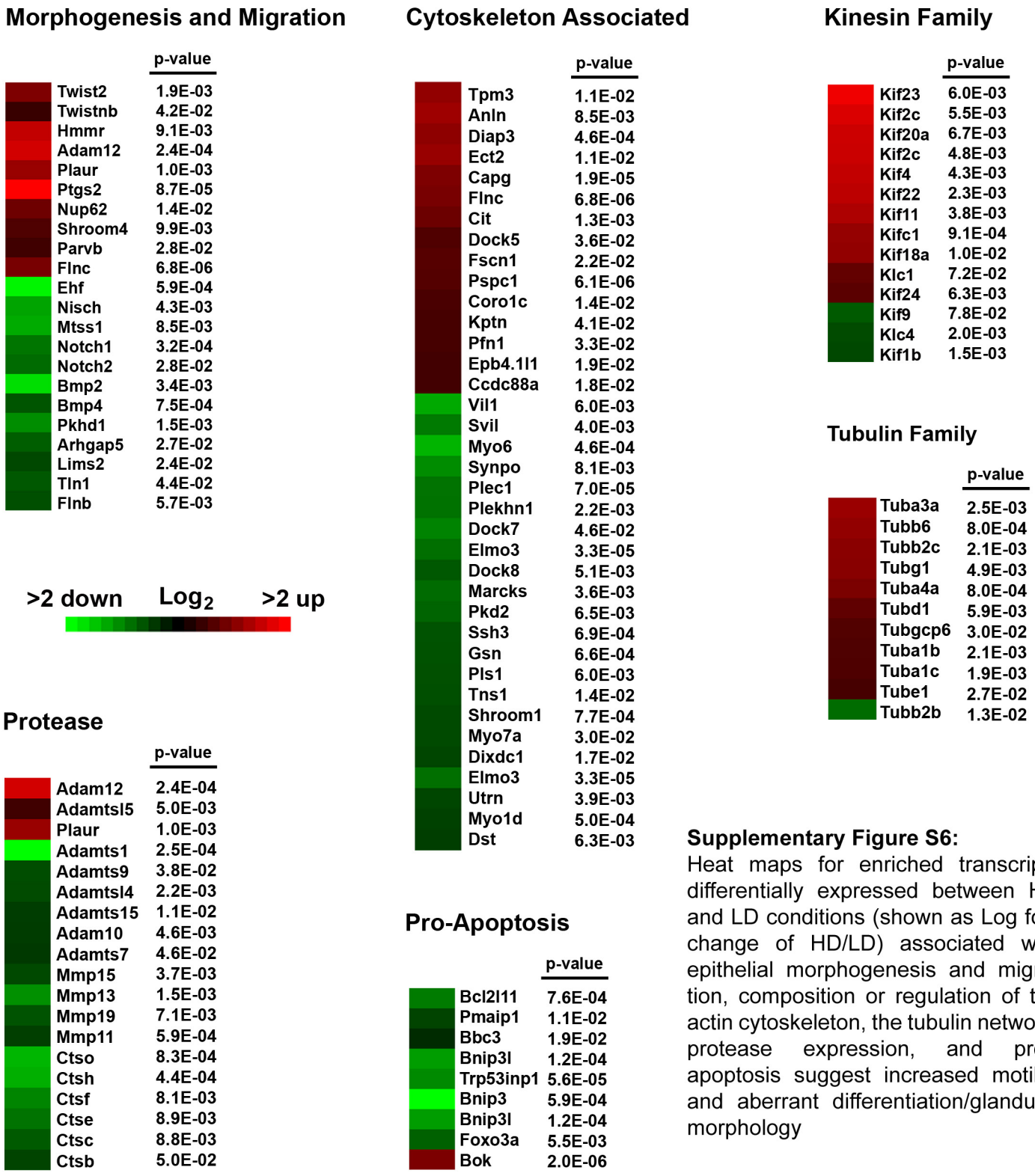

Supplementary Figure S6:
Heat maps for enriched transcripts differentially expressed between HD and LD conditions (shown as Log fold change of HD/LD) associated with epithelial morphogenesis and migration, composition or regulation of the actin cytoskeleton, the tubulin network, protease expression, and pro-apoptosis suggest increased motility and aberrant differentiation/glandular morphology

Provenzano et al., Supp. Figure S7

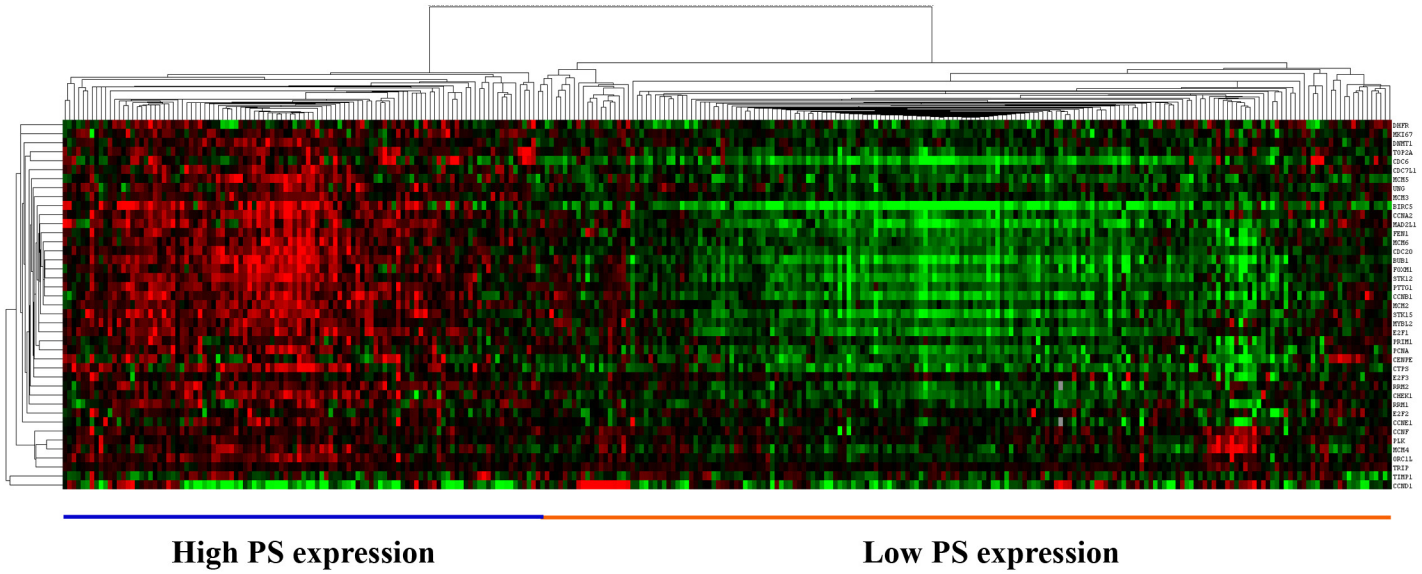

High PS expression **Low PS expression**

Supplementary Figure S7:
Hierarchical cluster of microarray data from breast cancer patients (columns; publically available data from van de Vijver et al., 2002) using the 41 genes associated with the conserved human breast cancer Proliferation Signature. Red and green indicate relatively high and low levels of expression, respectively. The transcripts divide breast cancer patients into two clusters, which correspond to the groups on the Kaplan-Meier curve shown in Figure 5 (the left patient cluster is shown in blue and the right cluster in orange in Kaplan-Meier graphs in Figure 5).

Provenzano et al., Supp. Figure S8

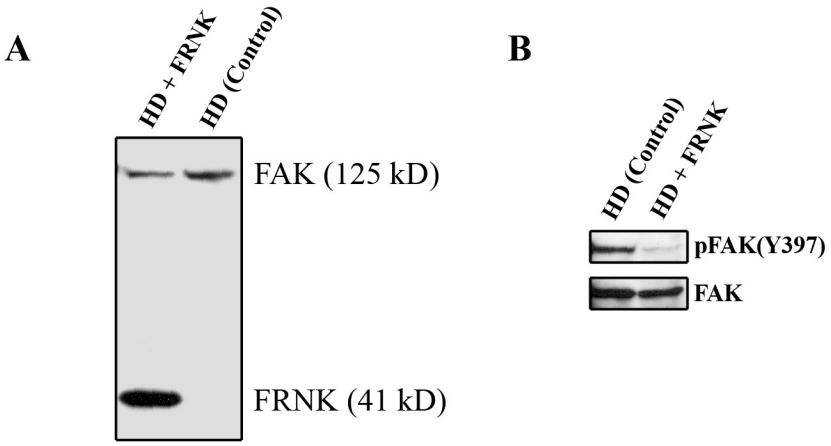

Supplementary Figure S8:
(A) Western blot of Control (ad-GFP) and FRNK (ad-GFP-FRNK) expressing NMuMG cells in HD matrices, probed with an antibody recognizing the C-terminal region of FAK. Note that FRNK is not GFP tagged, but GFP is expressed by a separate promoter in the viral vector in order to examine infection efficiency.
(B) Western blot of Control (ad-GFP) and FRNK (ad-GFP-FRNK) expressing NMuMG cells in HD matrices showing decreased phosphorylation of FAK at Y397 in cells expressing the dominant negative (FRNK).

Provenzano et al., Supp. Figure S9

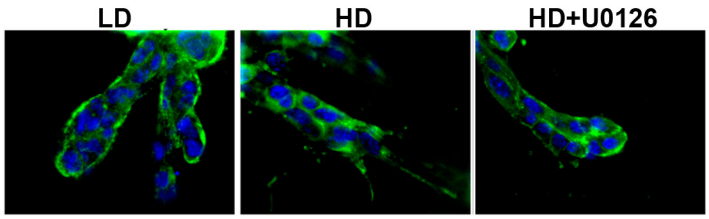

Supplementary Figure S7: Color version of figure 7E

SUPPLEMENTARY MATERIALS AND METHODS

3D Cell Culture

Human MCF10A T47D, and MDA-MB-231 mammary epithelial cells were maintained as described previously [1,2]. Non-immortalized normal murine mammary gland (NMuMG) cells (a gift from Dr. Caroline Alexander, University of Wisconsin) were maintained in DMEM supplemented with 10% (v/v) FBS and 10 μg/ml insulin. For 3D culture, cells were placed into 1.3-4.0 mg/mL collagen gels (BD Biosciences) that were neutralized with 2X HEPES buffer and culture media. Following collagen matrix polymerization for 16 hours the gels were released from the culture dish and floated in cell appropriate media to allow free gel contraction unless otherwise noted in the text. Media was changed every 4 days. Note that mammary epithelial cells in collagen matrices express and organize their own laminin- and collagen IV-containing basement membrane (data not shown). Moreover, cell type had an optimal collagen density for promoting tubulogenesis that was determined through preliminary experiments in which each cell type was cultured in collagen matrices ranging in density from 1.0-5.0 mg/mL. The optimal density for normal growth and differentiation is designated LD (for low-density) and were compared to HD (high density) conditions that disrupted normal differentiation. Conditions for each cell type used in morphogenesis assays were as follows: MCF10A and T47D (LD = 1.3mg/mL; HD = 3.0 mg/mL), NMuMG (LD = 3.0 mg/mL; HD = 4.0 mg/mL).

Inhibitors, Infections, and Transfections

Inhibitors used in this study were C3 exoenzyme (10 μg/mL; Cytoskeleton), H1152 (a more potent and selective inhibitor than Y27632; 2.5 μM), blebbistatin (a nonmuscle myosin ATPase inhibitor; 10 μM), and cytochalasin D (1 μM) all from Calbiochem, and U0126 (10 μM; Promega). Infection with adenovirus (Ad-GFP, Ad-FRNK-GFP - a C-terminal region of FAK that acts in a dominant-negative

manner, and dominant-negative Ad-Rho(N19)-GFP, which were a gift from Dr. Christopher S. Chen, Univ. of Pennsylvania) were performed as described previously [3]. siRNA oligonucleotides targeting murine FAK (target sequence: AACCACCTGGGCCAGTATTAT) or providing a non-silencing control sequence (target sequence: AATTCTCCGAACGTGTCACGT), with no homology to any known mammalian mRNA, were synthesized by Qiagen (Germantown, MD). siRNAs or GFP-vinculin were transfected with Lipofectamin 2000 (Invitrogen) following the manufacturer's directions. For experiments involving single cells, siRNA was labeled with Cy3 using the Ambion Silencer® siRNA labeling kit according to the manufacturer's directions.

Xenograft experiments

Mice were maintained at the University of Wisconsin under the approval and guidelines of the Institutional Animal Care and Use Committee. MDA-MB-231 cells were seeded into low density (LD: 1.0 mg/mL) and high density (HD: 3.0 mg/mL) collagen matrix plugs in 48-well plates at a density of $5*10^5$ cells/plug. Collagen matrices were then implanted into female athymic nude mice (BALB/c *nu/nu* mice, Charles River Laboratories). Collagen matrices were transplanted above the 4^{th} inguinal mammary glands, with each mouse receiving a LD and HD matrix. After initial tumor formation, tumor size was measured every 3-4 days. Tumor volume was calculated as $3/4\pi r^3$.

Preparation of polyacrylamide substrates

Polyacrylamide substrates were prepared as described by Pelham and Wang (1997) and Yeung et al., (2005). This system allowed us to study MECs as they sense and respond to changes in the mechanical properties of their microenvironment. Herein, rigidity of 10% (w/v) acyrlamide substrates was modulated by varying the concentration of bisacrylamide cross-linker from 0.1-0.4% (w/v), and polymerization was induced with ammoniumpersulfate and N,N,N,N-Tetramethylethylenediamine. Following UV photoactivation with Sulfo-SANPAH to crosslink extracellular matrix to the gel surface, gels were coated

with 30 μg/mL type I collagen. Shear modulus values were obtained by interpolating the data of Yeung and co-workers, which showed that for acrylamide concentrations greater than 7.5% the modulus scales linearly with cross-linker concentration [4].

Multiphoton Laser-Scanning Microscopy (MPLSM)

Multiphoton excitation and second harmonic generation imaging microscopy were performed as previously described [1,5]. Live cell and collagen imaging was performed with MPLSM to generate multiphoton excitation (MPE) and second harmonic generation (SHG). The system employs a mode-locked Ti:sapphire laser (Millennium/Tsunami, Spectra-Physics, Mountain View, CA) excitation source producing around 100fs pulse widths, which was tuned to 890 nm to simultaneously generate MPE of GFP-Vinculin and second harmonic generation (SHG) signal from collagen. The beam was focused onto the sample with a Nikon 60X Plan Apo water-immersion lens (NA = 1.2). Since SHG is not a fluorescent process and as such has no lifetime (see [6]), the presence of collagen was confirmed using fluorescence lifetime imaging microscopy (FLIM) on the same system. Furthermore, due to the fundamentally different physical properties of MPE and SHG, signals could be discriminated by filtering the emission signal. We used a 480-550 nm (band-pass) filter to isolate the MPE emission from GFP and a 445 nm narrow-band pass filter to isolate SHG signal (all filters: TFI Technologies, Greenfield, MA).

Material property measurements

Mechanical testing to generate stress-strain curves and modulus calculation for collagen matrices was performed as described previously [7] using sample design and handling similar to that described by Roeder and co-workers [8]. The relationship between elastic modulus (E) and shear modulus (G) was assumed to be governed as $E=2G(1+\nu)$, where ν is Poisson's ratio.

Cell / Matrix deformation

For cell deformation on 2D surfaces, 10^5 mammary epithelial cells were plated onto type I collagen coated 6-well plates (Bioflex Plates, Flexcell Corp.) for 24 hours, in cell specific media (as described above), which was sufficient for cell attachment. A static tensile equibiaxial strain (10%) was applied to the substrate for 20 minutes with a FlexCell® apparatus in an incubator at 37º C with 5% CO_2. Control cells were mounted in the loading frame alongside loaded cells, but no load was applied to the control plates. For tensile loading of 3D collagen matrices, mammary epithelial cells were seeded into matrices formed within Flexcell TissueTrain® culture plates. Uniaxial tensile strain (10%) was applied to the cell-seeded collagen matrices for 20 minutes in an incubator at 37º C with 5% CO_2.

Immunofluorescence

Immunofluorescence microscopy of cells in or on 3D matrices was performed as described previously [5]. Primary antibodies: FAK 4.47 mAb (Upstate); FAK phospho-specfic FAK(Y397) pAb and Src Y418 pAb (Biosource); ACTIVE® ERK1/2 pAb (Promega); Vinculin mAb (Sigma); Paxillin mAb (Transduction Labs). Cell proliferation was examined by using anti-Ki-67 (mouse clone 7B11 (Zymed) for human cells and a goat polyclonal Ab (Santa Cruz) for mouse cells. Anti-rabbit or –mouse secondary antibodies conjugated to either FITC or TRITC (Jackson ImmunoResearch Laboratories), FITC-conjugated phalloidin (Sigma), and bisbenzimide (Sigma) were used as secondary reagents.

Morphometric Analysis

Quantitative analysis of cell morphology was performed in ImageJ (http://rsb.info.nih.gov/ij/). To quantify membrane protrusion into the ECM, two morphological indices were generated. Protrusion length and membrane perimeter were measured for single cells in mammary epithelial colonies that developed in LD and HD matrices. Cells at the leading edge of colony branches, at the cell-matrix

interface, were examined. First, membrane perimeter was quantified by calculating the nucleus centroid in equalized threshold images and defining the ECM-facing half of the cells as a region of interest in which the cell membrane perimeter was measured (see sample illustration below). To quantify membrane protrusion length, the three longest membrane distances from the nucleus centroid (within a region defined by two perpendicular lines that were each 45 degrees from the bisecting line that passed through the centroidal midline of the nucleus) that were at least 15 degrees apart were measured. Note that analyzed images were extracted from z-stacks through the 3D epithelial structures and the quantification of perimeter and length was made in the optical plane containing in focus 3D matrix adhesions that were at or near the longest protrusion length. However, due to the 3D nature of the cellular structures, morphometric analysis in a 2D optical section can underestimate the true maximum protrusion length. Nevertheless, analysis herein is comparative between 3D structures and examination of the z-stacks did not suggest large angles between protrusion primary axes and the optical plane. Furthermore, correction for any such angles in long protrusions present in cells within HD matrices would further enhance the length difference between cells in LD and HD matrices. To determine FA area, images were normalized

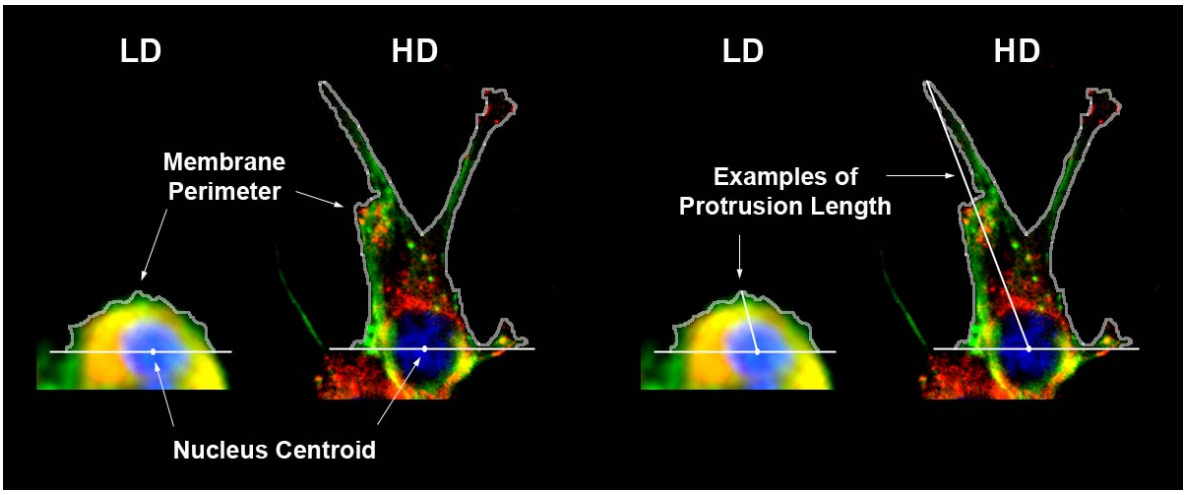

Example illustrations of morphometric analyses used in this study.

and the threshold limited area of each adhesion measured within 10 μm of the cell perimeter.

Immunoprecipitation and Western blotting

Cells in 3D matrices were lysed in an equal volume of 2X solution to produce a final 1X mixture of 10mM Tris, 100mM NaCl, 1mM EDTA, 1mM EGTA, 1mM NaF, 20 mM $Na_4P_2O_7$, 2mM $NaVO_4$, 1% Triton X-100, 10% Glycerol, 0.1% SDS, 0.5% deoxychlate, 1mM PMSF, and protease inhibitor cocktail (Set III; Calbiochem), for direct Western blotting and all immunoprecipitation experiments. Immunoprecipitation was performed on cleared lysates at 4ºC using 4 μg of antibody (FAK C-20 pAb (Santa Cruz) or 4.47 mAb (Upstate), Src mAb (Upstate), or species-specific control IgG antibodies in co-immunoprecipitation experiments) and 30 μl of Gammabind beads (Amersham Biosciences) per matrix sample. After washing, the samples were prepared for SDS-PAGE with the addition of Laemli buffer. Western blotting was performed as described previously [3]. For immunoblotting, membranes were incubated with the following primary antibodies: Upstate: anti-FAK 4.47, anti-Src; Biosource: anti-FAK(Y397) or (Y925), anti-Src(Y418); Santa Cruz: pY99, pY350, anti-GAPDH; Promega: anti-ACTIVE ERK1/2, anti-ERK1/2; Transduction Labs: anti-SHC and anti-Grb2. HRP-conjugated secondary antibodies (Jackson Laboratories) were used.

Rho GTPase Activation Assay

Rho-A activity was determined using an ELISA based assay (G-LISA^{TM} Luminometric Rho-A assay, Cytoskeleton) according to the manufacture's direction, with the following exception. The lysate volume loaded into each well was increased ≥3-fold to overcome signal loss due to a less concentrated sample obtained from 3D matrices (as compared to a more concentrated sample from cells on 2D culture plates).

RNA Isolation and Microarray

Total RNA was isolated from mammary epithelial cells in 3D collagen matrices (LD, n=5; HD, n=5; HD+DMSO, n=5; HD+U0126, n=5) in manner similar to a previous report [3]. Briefly, multiple matrices

(n=6) were pooled for each condition (i.e. one sample above is composed of six cell-seeded matrices) to increase statistical power [9]. Samples were lysed with TRIzol reagent (Invitrogen), separated with heavy-phase lock gel (Eppendorf), and further purified using RNeasy columns with DNAse digest (Qiagen). Total RNA quantity and purity were analyzed with a NanoDrop® ND-1000 Spectrophotometer. RNA quality was analyzed by acrylamide-gel electrophoresis, and quality and quantity confirmed using Agilent 2100 BioAnalyzer chips. All RNA was of high quality and appropriate quantity. RNA samples were then prepared for hybridization and hybridized to Affymetrix 430 2.0 mouse arrays at the UW-Madison – Gene Expression Center.

Data Analysis and Bioinformatics

GC-RMA normalization, statistical analysis, and principal component analysis (PCA) were performed with ArrayAssist (Stratagene). Gene ontology analysis was performed using the ArrayAssist GO browser and/or the Database for Annotation, Visualization and Integrated Discovery, or DAVID [10]. Cluster and Java-Treeview was used to execute and visualize hierarchical clustering, respectively. For cluster analysis of human breast tumors, the publicly available gene expression data from van de Vijver et al., [11] was utilized. Toucan [12] was used to computationally determine enriched transcription factor binding sites (TFBS) within select gene lists. Promoter sequences 0.5 kb upstream and 0.1 kb downstream of the transcriptional start site were analyzed with MotifScanner using the TRANSFAC database (Public 7.0 Vertebrates). The mouse 1kb Proximal 1000 ENSMUSG (3) background model was used with a 0.1 stringency level. Statistically over-represented binding sites were generated relative to the appropriate expected frequency file for mouse. *Prob* represents the probability of finding more than *n* (the number of times the TF site appears) occurrences within the sequences, while the *Sig Value (S)* represents the number of random patterns once expects to find following the relation 10^S (e.g. $S = 3$ would indicate one random pattern in every 1000 families and so on; for more information see [12] and tutorials listed therein). The complete lists of enriched TFBS are available upon request.

Statistical Analysis

Two-group data were analyzed with t-tests. Analysis of Variance (ANOVA) followed by the Tukey-Kramer multiple comparison test was used for multi-group data. Clinical survival data was compared using the Logrank test.

References

1. Provenzano PP, Inman DR, Eliceiri KW, Trier SM, Keely PJ (2008) Contact guidance mediated 3D cell migration is regulated by Rho/ROCK-dependent matrix reorganization. Biophys J.
2. Wozniak MA, Desai R, Solski P, Der CJ, Keely PJ (2003) ROCK-generated contractility regulates breast epithelial cell differentiation in response to physical properties of a three-dimensional collagen matrix. Journal of Cell Biology 163: 583-595.
3. Provenzano PP, Inman DR, Eliceiri KW, Beggs HE, Keely PJ (2008) Mammary Epithelial-Specific Disruption of Focal Adhesion Kinase Retards Tumor Formation and Metastasis in a Transgenic Mouse Model of Human Breast Cancer. American Journal of Pathology 173: 1551-1565.
4. Yeung T, Georges PC, Flanagan LA, Marg B, Ortiz M, et al. (2005) Effects of substrate stiffness on cell morphology, cytoskeletal structure, and adhesion. Cell Motil Cytoskeleton 60: 24-34.
5. Provenzano PP, Inman DR, Eliceiri KW, Knittel JG, Yan L, et al. (2008) Collagen density promotes mammary tumor initiation and progression. BMC Med 6: 11.
6. Provenzano PP, Eliceiri KW, Keely PJ (2008) Multiphoton microscopy and fluorescence lifetime imaging microscopy (FLIM) to monitor metastasis and the tumor microenvironment. Clin Exp Metastasis.
7. Provenzano PP, Martinez DA, Grindeland RE, Dwyer KW, Turner J, et al. (2003) Hindlimb unloading alters ligament healing. J Appl Physiol 94: 314-324.
8. Roeder BA, Kokini K, Sturgis JE, Robinson JP, Voytik-Harbin SL (2002) Tensile mechanical properties of three-dimensional type I collagen extracellular matrices with varied microstructure. J Biomech Eng 124: 214-222.
9. Kendziorski C, Irizarry RA, Chen K-S, Haag JD, Gould MN (2005) On the utility of pooling biological samples in microarray experiments. PNAS 102: 4252-4257.
10. Dennis G, Jr., Sherman BT, Hosack DA, Yang J, Gao W, et al. (2003) DAVID: Database for Annotation, Visualization, and Integrated Discovery. Genome Biol 4: P3.
11. van de Vijver MJ, He YD, van't Veer LJ, Dai H, Hart AA, et al. (2002) A gene-expression signature as a predictor of survival in breast cancer. N Engl J Med 347: 1999-2009.
12. Aerts S, Thijs G, Coessens B, Staes M, Moreau Y, et al. (2003) Toucan: deciphering the cis-regulatory logic of coregulated genes. Nucleic Acids Res 31: 1753-1764.

Supplementary Discussion Text:

The role of FAK in response to density-induced matrix stiffness

Both application of exogenous force, and culture in stiff 3D collagen matrices promoted hyper-activation of FAK, evidenced by increased phosphorylation at both Y397 and Y925 (as well as phosphorylation within the kinase domain at Y576/577; data not shown) in non-transformed mammary epithelial cells. This is consistent with previous reports that show increased FAK Y397 phosphorylation resulting from culturing mammary epithelial cells on stiff basement membrane gels (Paszek et al., 2005) or culturing transformed T47D cells in collagen matrices of increasing density (Wozniak et al., 2003). In addition, FAK has recently been shown to be necessary for local invasion and pulmonary metastasis (Lahlou et al., 2007; Mitra et al., 2006; Provenzano et al., 2008) and both high breast tissue density and FAK overexpression correlate with more aggressive and invasive human breast carcinomas (Gill et al., 2006; Habel et al., 2004; Lark et al., 2005). As such, one might reasonably speculate that the increased stiffness associated with breast adenomas and carcinomas (Sarvazyan et al., 1995; Sumi et al., 2000) and/or high collagen density is promoting FAK activation *in vivo* to support invasive tumor cell behavior, which is consistent with increased FAK phosphorylation in invasive MDA-MB-231 breast carcinoma cells following application of force (see Fig 3A) and increased growth *in vivo* in HD matrices (see Fig 6B). Furthermore, while increased levels of activated FAK have not been shown to directly promote mammary epithelial growth *in vivo,* FAK is overexpressed in numerous human cancers. Significantly, loss of FAK has been shown to inhibit growth in transgenic models of human breast cancer (Lahlou et al., 2007; Provenzano et al., 2008). As such, in relation to 'normal' epithelial cells in collagen dense breasts, our results suggest that in response to increased collagen density, chronic hyperactivation of FAK-

mediated signaling may be part of the mechanism by which epithelial cells react to high breast tissue density, which results in excessive growth and disrupts normal tissue architecture.

Gill, J.K., Maskarinec, G., Pagano, I. & Kolonel, L.N. (2006). *Breast Cancer Res*, **8,** R30.

Habel, L.A., Dignam, J.J., Land, S.R., Salane, M., Capra, A.M. & Julian, T.B. (2004). *J Natl Cancer Inst*, **96,** 1467-72.

Lahlou, H., Sanguin-Gendreau, V., Zuo, D., Cardiff, R.D., McLean, G.W., Frame, M.C. & Muller, W.J. (2007). *Proc Natl Acad Sci U S A*, **104,** 20302-7.

Lark, A.L., Livasy, C.A., Dressler, L., Moore, D.T., Millikan, R.C., Geradts, J., Iacocca, M., Cowan, D., Little, D., Craven, R.J. & Cance, W. (2005). *Mod Pathol*, **18,** 1289-94.

Mitra, S.K., Lim, S.T., Chi, A. & Schlaepfer, D.D. (2006). *Oncogene*, **25,** 4429-40.

Paszek, M.J., Zahir, N., Johnson, K.R., Lakins, J.N., Rozenberg, G.I., Gefen, A., Reinhart-King, C.A., Margulies, S.S., Dembo, M., Boettiger, D., Hammer, D.A. & Weaver, V.M. (2005). *Cancer Cell*, **8,** 241-54.

Provenzano, P.P., Inman, D.R., Eliceiri, K.W., Beggs, H.E. & Keely, P.J. (2008). *American Journal of Pathology*, **173,** 1551-65.

Sarvazyan, A.P., Skovaroda, A.R., Emelianov, S.Y., Fowlkes, J.B., Pipe, J.G., Adler, R.S., Buxton, R.B. & Carson, P.L. (1995). *Acoust. Imaging*, **21,** 223-240.

Sumi, C., Nakayama, K. & Kubota, M. (2000). *Phys Med Biol*, **45,** 1511-20.

Wozniak, M.A., Desai, R., Solski, P., Der, C.J. & Keely, P.J. (2003). *Journal of Cell Biology*, **163,** 583-595.